The Journal of Chemical Physics

Coulomb explosion imaging of CH_3I and CH_2ClI photodissociation dynamics

Cite as: J. Chem. Phys. **149**, 204313 (2018); https://doi.org/10.1063/1.5041381
Submitted: 24 May 2018 . Accepted: 19 October 2018 . Published Online: 30 November 2018

Felix Allum, Michael Burt, Kasra Amini, Rebecca Boll, Hansjochen Köckert, Pavel K. Olshin, Sadia Bari, Cédric Bomme, Felix Braußе, Barbara Cunha de Miranda, Stefan Düsterer, Benjamin Erk, Marie Géléoc, Romain Geneaux, Alexander S. Gentleman, Gildas Goldsztejn, Renaud Guillemin, David M. P. Holland, Iyas Ismail, Per Johnsson, Loïc Journel, Jochen Küpper, Jan Lahl, Jason W. L. Lee, Sylvain Maclot, Stuart R. Mackenzie, Bastian Manschwetus, Andrey S. Mereshchenko, Robert Mason, Jérôme Palaudoux, Maria Novella Piancastelli, Francis Penent, Dimitrios Rompotis, Arnaud Rouzée, Thierry Ruchon, Artem Rudenko, Evgeny Savelyev, Marc Simon, Nora Schirmel, Henrik Stapelfeldt, Simone Techert, Oksana Travnikova, Sebastian Trippel, Jonathan G. Underwood, Claire Vallance, Joss Wiese, Farzaneh Ziaee, Mark Brouard, Tatiana Marchenko, and Daniel Rolles

View Online Export Citation CrossMark

ARTICLES YOU MAY BE INTERESTED IN

Photodissociation of aligned CH_3I and $C_6H_3F_2I$ molecules probed with time-resolved Coulomb explosion imaging by site-selective extreme ultraviolet ionization
Structural Dynamics **5**, 014301 (2018); https://doi.org/10.1063/1.4998648

Communication: Gas-phase structural isomer identification by Coulomb explosion of aligned molecules
The Journal of Chemical Physics **148**, 091102 (2018); https://doi.org/10.1063/1.5023441

Velocity map imaging of ions and electrons using electrostatic lenses: Application in photoelectron and photofragment ion imaging of molecular oxygen
Review of Scientific Instruments **68**, 3477 (1997); https://doi.org/10.1063/1.1148310

Lock-in Amplifiers up to 600 MHz
Watch

© 2018 Author(s).

Coulomb explosion imaging of CH_3I and CH_2ClI photodissociation dynamics

Felix Allum,[1] Michael Burt,[1] Kasra Amini,[1] Rebecca Boll,[2] Hansjochen Köckert,[1] Pavel K. Olshin,[3] Sadia Bari,[2] Cédric Bomme,[2] Felix Braußе,[4] Barbara Cunha de Miranda,[5] Stefan Düsterer,[2] Benjamin Erk,[2] Marie Géléoc,[6] Romain Geneaux,[6] Alexander S. Gentleman,[7] Gildas Goldsztejn,[4] Renaud Guillemin,[5] David M. P. Holland,[8] Iyas Ismail,[5] Per Johnsson,[9] Loïc Journel,[5] Jochen Küpper,[10,11,12,13] Jan Lahl,[9] Jason W. L. Lee,[1] Sylvain Maclot,[9] Stuart R. Mackenzie,[7] Bastian Manschwetus,[2] Andrey S. Mereshchenko,[3] Robert Mason,[1] Jérôme Palaudoux,[5] Maria Novella Piancastelli,[5,14] Francis Penent,[5] Dimitrios Rompotis,[2,15] Arnaud Rouzée,[4] Thierry Ruchon,[6] Artem Rudenko,[16] Evgeny Savelyev,[2] Marc Simon,[5] Nora Schirmel,[2] Henrik Stapelfeldt,[17] Simone Techert,[2,18,19] Oksana Travnikova,[5] Sebastian Trippel,[10,11] Jonathan G. Underwood,[20] Claire Vallance,[1] Joss Wiese,[10,13] Farzaneh Ziaee,[16] Mark Brouard,[1,a)] Tatiana Marchenko,[5] and Daniel Rolles[16]

[1]*The Chemistry Research Laboratory, Department of Chemistry, University of Oxford, Oxford OX1 3TA, United Kingdom*
[2]*Deutsches Elektronen-Synchrotron DESY, Notkestraße 85, 22607 Hamburg, Germany*
[3]*Saint-Petersburg State University, 7/9 Universitetskaya nab., St. Petersburg 199034, Russia*
[4]*Max-Born-Institut, Max-Born-Straße 2A, 12489 Berlin, Germany*
[5]*Sorbonne Université, CNRS, Laboratoire de Chimie Physique—Matière et Rayonnement, LCPMR, F-75005 Paris, France*
[6]*LIDYL, CEA, CNRS, Université Paris-Saclay, CEA-Saclay, 91191 Gif-sur-Yvette, France*
[7]*The Physical and Theoretical Chemistry Laboratory, Department of Chemistry, University of Oxford, Oxford OX1 3QZ, United Kingdom*
[8]*Daresbury Laboratory, Daresbury, Warrington, Cheshire WA4 4AD, United Kingdom*
[9]*Department of Physics, Lund University, 22100 Lund, Sweden*
[10]*Center for Free-Electron Laser Science, Deutsches Elektronen-Synchrotron DESY, Notkestraße 85, 22607 Hamburg, Germany*
[11]*Center for Ultrafast Imaging, Universität Hamburg, Luruper Chaussee 149, 22761 Hamburg, Germany*
[12]*Department of Physics, Universität Hamburg, Luruper Chaussee 149, 22761 Hamburg, Germany*
[13]*Department of Chemistry, Universität Hamburg, Martin-Luther-King-Platz 6, 20146 Hamburg, Germany*
[14]*Department of Physics and Astronomy, Uppsala University, P.O. Box 516, 75120 Uppsala, Sweden*
[15]*European XFEL, Holzkoppel 4, 22869 Schenefeld, Germany*
[16]*J. R. Macdonald Laboratory, Department of Physics, Kansas State University, Manhattan, Kansas 66506, USA*
[17]*Department of Chemistry, Aarhus University, Langelandsgade 140, DK-8000 Aarhus C, Denmark*
[18]*Max Planck Institute for Biophysical Chemistry, 37077 Göttingen, Germany*
[19]*Institute of X-ray Physics, University of Göttingen, 37077 Göttingen, Germany*
[20]*Department of Physics and Astronomy, University College London, London WC1E 6BT, United Kingdom*

(Received 24 May 2018; accepted 19 October 2018; published online 30 November 2018)

The photodissociation dynamics of CH_3I and CH_2ClI at 272 nm were investigated by time-resolved Coulomb explosion imaging, with an intense non-resonant 815 nm probe pulse. Fragment ion momenta over a wide *m*/*z* range were recorded simultaneously by coupling a velocity map imaging spectrometer with a pixel imaging mass spectrometry camera. For both molecules, delay-dependent pump-probe features were assigned to ultraviolet-induced carbon-iodine bond cleavage followed by Coulomb explosion. Multi-mass imaging also allowed the sequential cleavage of both carbon-halogen bonds in CH_2ClI to be investigated. Furthermore, delay-dependent *relative* fragment momenta of a pair of ions were directly determined using recoil-frame covariance analysis. These results are complementary to conventional velocity map imaging experiments and demonstrate the application of time-resolved Coulomb explosion imaging to photoinduced real-time molecular motion. *Published by AIP Publishing.* https://doi.org/10.1063/1.5041381

I. INTRODUCTION

The development of ultrashort laser pulses has facilitated a wide range of studies on chemical reactions on the femtosecond scale of nuclear motion.[1] Molecules rapidly ionize when exposed to intense ultrashort pulses ($>10^{14}$ W cm^{-2}),[2] and the resulting polycations, which are unstable with respect to Coulomb explosion, fragment into several ions.[3] If the explosion occurs prior to any rearrangement of the parent cation, the momenta of the resulting fragments are sensitive

a)Electronic mail: mark.brouard@chem.ox.ac.uk

to the structure of the original neutral molecule.[3,4] This phenomenon, termed Coulomb explosion imaging (CEI), has been used to determine the structures of neutral molecules in the gas phase.[3–7] By coupling CEI with ultrafast pump-probe spectroscopy, it is possible to initiate Coulomb explosion at a range of delays following the pump pulse and in doing so monitor the evolution of the structural dynamics initiated by the pump pulse in "real time."[8–16] In this study, time-resolved CEI is used to study the photodissociation of the halomethane CH_3I and dihalomethane CH_2ClI. The experimental results are also compared with similar research recently carried out on CH_2BrI in order to explore the relationship between the photochemistry of these similar molecules.[17]

The ultraviolet photodissociation of CH_3I in its *A*-band has been thoroughly studied both theoretically and experimentally[18–27] and is a model system for understanding photofragmentation in the gas phase. The analogous photodissociation of CH_2ClI has been the subject of fewer studies.[28–32] Absorption by CH_3I in its *A*-band (220-350 nm) arises due to excitations to three repulsive electronic states, as depicted in Fig. 1. The dominant transition at the wavelength used in this study (272 nm) is to the $^3Q_0$ state, which leads to direct C-I bond cleavage into a methyl radical and a spin-orbit excited iodine atom ($^2P_{1/2}$).[23] The other significant pathway from the $^3Q_0$ state is a dissociation to a ground state iodine ($^2P_{3/2}$), which occurs via a curve crossing to the $^1Q_1$ state.[23] Both pathways have been well studied using ion-imaging at a range of excitation wavelengths, yielding kinetic energy releases (KERs), anisotropy parameters, and branching ratios.[21,23,33–36]

The dihalomethane CH_2ClI exhibits more complex and varied dynamics in the ultraviolet (UV), with each carbon-halogen bond acting as a separate chromophore.[30] At different wavelengths, preferential dissociation of either halogen atom can be observed,[30] as well as the elimination of ICl.[29–32,37] Similar multi-pathway chemistry is also exhibited by CH_2BrI.[38,39] The excitation wavelength used in this study (272 nm) lies near the centre of the *A*-band of CH_2ClI (225-325 nm). This band arises due to the excitation of a non-bonding electron located on the iodine atom (n) to the C–I antibonding orbital (σ^*) and is red-shifted with respect to the corresponding CH_3I band due to stabilization of the C–I σ^* by the chlorine atom. Excitation in this band is predominantly followed by cleavage of the C–I bond to produce iodine radicals in either their ground or excited spin-orbit state.[29]

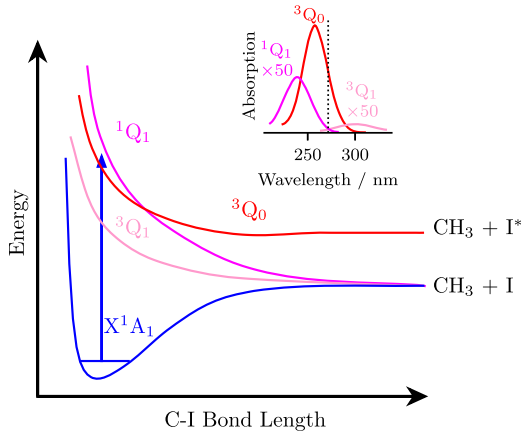

FIG. 1. Potential energy curves for iodomethane showing the relevant electronic states at 272 nm. The decomposed absorption spectrum (inset) is also shown, with the position of 272 nm marked with a dotted line. Excitation is primarily to the $^3Q_0$ state, which is dissociative and correlates to methyl and I^* ($^2P_{1/2}$) radicals. Methyl radicals paired with a ground state I ($^2P_{3/2}$) are produced following a non-adiabatic curve crossing to the $^1Q_1$ state. Adapted from Ref. 25.

In this paper, the dissociations of the C–I bond in CH_3I and CH_2ClI are studied on a femtosecond time scale using time-resolved CEI, focusing on the delay-dependent kinetic energy releases of characteristic fragment ions. This allows effects attributable to the known photochemical behaviors of these molecules to be assigned and confirmed by classical simulations. The data also agree with the literature values obtained using resonance enhanced multiphoton ionization (REMPI) schemes.[23,28] In the case of CH_3I, time-dependent features arising from different iodine product quantum states were well-resolved and characterised, whilst in CH_2ClI, dissociation processes involving cleavage of both carbon-halogen bonds were probed within a single experiment. Time-resolved covariance analysis is used to show how the relative momenta of a pair of ions evolve as a function of pump-probe delay. Between the molecules studied here and CH_2BrI studied previously,[17] differences in the internal energy distribution following photodissociation were observed and attributed to the structural influence of the halogen atoms. The results provide promising support for the use of CEI coupled with covariance analysis as a universal probe of photon-induced dynamics which could be applied to larger molecular systems and more complex reactions, such as molecular isomerisation.

II. EXPERIMENTAL METHODS

Experiments were carried out at the CAMP multipurpose instrument at the free-electron laser in Hamburg (FLASH).[40–42] The CAMP instrument offers a double-sided velocity map imaging (VMI) spectrometer that allows for the simultaneous velocity mapping of fragment ions and photoelectrons and has been described in detail elsewhere.[43] Briefly, each molecule was evaporated at room temperature and introduced into the spectrometer through two skimmers as a continuous jet. The collimated molecular beam was then intersected perpendicularly in the VMI interaction region by the frequency tripled pump (λ = 272 nm, 2.5 nm FWHM bandwidth) and the fundamental probe (λ = 815 nm, 26 nm FWHM bandwidth) output of the FLASH optical laser. Fundamental infrared (IR) pulses of 55 fs duration were generated using a 10 Hz Ti:sapphire oscillator and a chirped pulse amplifier.[44] UV pulses were produced by splitting the IR beam and passing it through a 50 μm thick frequency tripling crystal on a 1 mm substrate, followed by a prism compressor. Typical IR and UV pulse energies were 1.22 mJ and 95 μJ, respectively, for the CH_3I experiments and 920 μJ and 63 μJ for the CH_2ClI experiments. The beams were focussed onto a 40×60 μm^2 spot in the interaction region. In order to observe the time-evolution of the dynamics induced by the UV pump pulse, the delay between the two pulses was varied using a computer-controlled delay stage.

Under velocity mapping conditions, positively charged fragments are accelerated such that ions with the same initial transverse velocity and mass-to-charge ratio (m/z) arrive at the same position on the two-dimensional detector,[45] which comprises two microchannel plates (MCPs) coupled to a P47 phosphor screen. During an experiment, several different ions are mapped onto the position-sensitive detector at their characteristic times-of-flight. The resulting flashes of light produced on the phosphor screen are imaged by a Pixel Imaging Mass Spectrometry (PImMS)[46,47] camera equipped with a PImMS2 sensor. This camera was synchronized to the 10 Hz pump-probe laser system, and several hundred frames were recorded per pump-probe delay.

PImMS2 is a 324 × 324 pixel detector capable of recording the position (x, y) and arrival times (t) of incident photons to a precision of 12.5 ns. This allows all fragment ions to be imaged in a single experimental cycle, over a wide m/z range. By recording all fragment momenta in one experiment, data can be collected under coincidence or covariance conditions to identify meaningful correlations between different ions.[14,48–51] The flash of light resulting from a single ion hit is generally registered in multiple pixels of the PImMS2 sensor and across multiple sequential time bins. The images presented here were consequently centroided in order to improve the momentum resolution of the data.[52] The pBASEX[53] algorithm was also used to Abel invert and obtain full three-dimensional velocity distributions from the two-dimensional projected ion images.

On the other end of the doubled-sided spectrometer, photoelectrons were simultaneously imaged using an MCP stack and a P20 phosphor screen coupled to a commercial charge-coupled device (CCD) camera. The analysis and discussion of the resulting photoelectron spectra are beyond the scope of this manuscript.

III. RESULTS AND DISCUSSION

Figure 2 shows the time-of-flight spectra for CH_3I and CH_2ClI, accumulated over *ca.* 50 000 and 55 000 laser shots, respectively, across a range of pump-probe delays. In the CH_3I experiments, images were recorded over a pump-probe delay range of −0.48 ps to +1.52 ps in steps of 20 fs. For CH_2ClI, data were recorded from −1.0 ps to +10.1 ps in 100 fs steps. One colour background data were also recorded which showed that the probe pulse initiated significantly more ionization and fragmentation than the pump, with a further appreciable enhancement in the signal in the pump-probe data.

Ion images for any of the peaks in the time-of-flight spectrum may be obtained by integrating the (x, y) data over the peak's time-of-flight range. For different delays, images of key fragments are shown in Fig. 3, with the main time-dependent channels illustrated by arrows. In the CH_2ClI case, these features can be clearly seen in multiple fragments: I^+, CH_2Cl^+, Cl^+, and CH_2^+. For CH_3I, delay-dependent effects are observed in the CH_3^+ and I^+ fragments, but are far more clearly visible in the CH_3^+ images. This occurs due to conservation of momentum; the majority of the kinetic energy released following photodissociation or Coulomb explosion

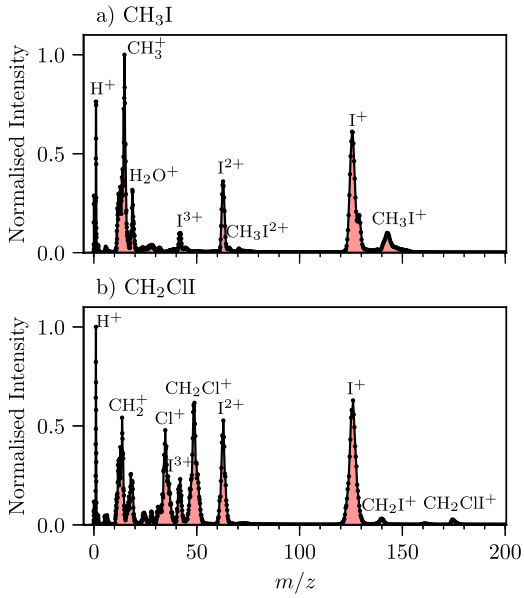

FIG. 2. Centroided time-of-flight spectra accumulated from the pump-probe delay scans for (a) CH_3I and (b) CH_2ClI. These have been normalised to the highest peak. Each data point represents a separate PImMS time bin and thus a separate ion image. It should be noted that due to the mass resolution of the experiment, ions differing by a small number of hydrogen atoms cannot be distinguished (e.g., CH_3^+ and CH_2^+).

is partitioned into the light methyl fragment, as opposed to the much heavier iodine. Additionally, images of heavier ions cover areas that are saturated by lighter, low kinetic energy background ions such as H_2O^+. This leads to visible "holes" in the images of the heavier ions. The position of time-zero was identified through cross correlation peaks in the yields of the high kinetic energy feature in I^+ and CH_3^+ for CH_3I and in

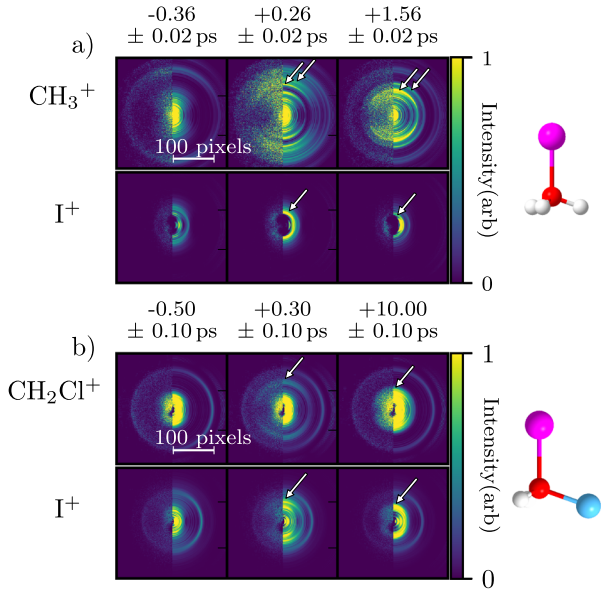

FIG. 3. Raw and pBASEX Abel inverted ion images at a series of pump-probe delays for (a) I^+ and CH_3^+ from CH_3I and (b) I^+ and CH_2Cl^+ from CH_2ClI. The delay-dependent features shrink with increasing delay and are highlighted with white arrows. Structures of the parent molecules are shown alongside the ion images. C, H, I, and Cl atoms are coloured red, gray, purple, and blue, respectively.

I^+ and CH_2Cl^+ for CH_2ClI. Cross correlations were typically ~280 fs (FWHM). Additionally, fitting the observed depletion of this feature after time-zero allowed us to estimate that 15-20% of molecules are excited by the pump pulse.

A. Iodomethane

1. Feature assignment

The time-dependent effects visible in Fig. 3 can be more clearly seen by plotting kinetic energies for each fragment as a function of delay time. Figure 4 illustrates this for the CH_3^+ fragment of CH_3I (little information can be gleaned from the corresponding map for the I^+ fragment, as discussed above). This was obtained by Abel inverting ion images at each delay step using the pBASEX algorithm,[53] normalizing by the number of frames, and then calibrating the radii to kinetic energies. This calibration was obtained by simulating trajectories in the spectrometer for ions with defined kinetic energies using SIMION.[54] Figure 4 shows a number of distinct features. The two features whose kinetic energy change with delay (labeled Ia and Ib) are assigned to photodissociation yielding a CH_3 radical partnered with an iodine atom either in its excited ($^2P_{1/2}$) or ground spin-orbit ($^2P_{3/2}$) state, followed by a Coulomb explosion (initiated by the probe pulse) between the CH_3^+ and the I^+ cofragments,

$$\text{Ia}: \quad CH_3I \xrightarrow{h\nu\ 272\,\text{nm}} CH_3 + I(^2P_{3/2}) \xrightarrow{nh\nu\ 815\,\text{nm}} CH_3^+ + I^+, \quad (1)$$

$$\text{Ib}: \quad CH_3I \xrightarrow{h\nu\ 272\,\text{nm}} CH_3 + I(^2P_{1/2}) \xrightarrow{nh\nu\ 815\,\text{nm}} CH_3^+ + I^+. \quad (2)$$

The Coulomb explosion contribution to the kinetic energy release decreases as the pump-probe delay increases, due to the increased distance between the two dissociating, neutral fragments at the time of ionization. Therefore, at sufficiently long delays, the energies of these channels should be solely due to the dissociation induced by the pump pulse. The energies of these channels at the longest delay time used in our experiment are 1.27 ± 0.08 eV and 1.96 ± 0.15 eV at + 1.52 ps, with uncertainties referring to the standard deviations of Gaussian fits of the kinetic energy spectrum. Subtracting the estimated Coulombic contribution from the kinetic energies (calculated using the simple classical model described later) gives 1.07 ± 0.08 eV and 1.80 ± 0.15 eV, in good agreement with the expected values of 1.05 eV and 1.83 eV, assuming the same energy partitioning as at 266 nm.[25]

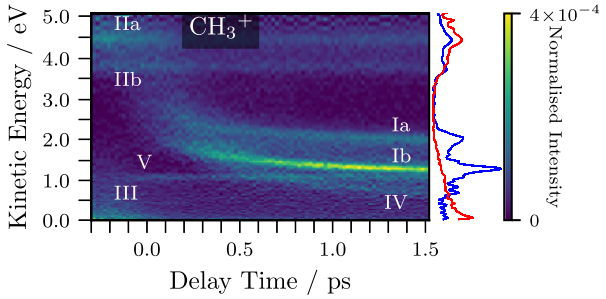

FIG. 4. The delay-dependent CH_3^+ kinetic energy distribution obtained from pBASEX Abel inverted ion images. Negative delays correspond to the IR probe pulse arriving first, and vice versa. The labeled features and their delay-dependence are discussed in detail in the main text. The kinetic energy spectrum for delays of +1.42 ps to +1.52 ps is projected to the right of the figure in blue. The kinetic energy spectrum for delays of −0.48 ps to −0.38 ps, in which the IR probe pulse arrives first, is projected in red.

By fitting Gaussian functions to the kinetic energy distributions of the two channels at individual delay bins, the relative intensity of the channels can be determined from the Gaussian peak areas. Assuming an equal ionization and detection probability of all CH_3 products, this allows for the I^*/I branching ratio to be determined directly from the CH_3^+ images. The calculated value of 0.64 ± 0.14 agrees reasonably well with the literature value of 0.73 (at an excitation wavelength of 266 nm) determined using REMPI detection of the two spin-orbit states of iodine.[23]

The high kinetic energy feature, which is split into two channels, labeled IIa and IIb in Fig. 4, is attributed to the (probe-only) Coulomb explosion of CH_3I molecules which have not dissociated prior to the arrival of the probe pulse. Assuming the charges induced prior to the explosion are located on the iodine and carbon atoms, the kinetic energy release of the static Coulomb explosion channel can be predicted using Coulomb's law. Taking the literature C–I bond distance of 214 pm[56] as the charge separation gives a kinetic energy of 6.02 eV for the CH_3^+ fragment, significantly greater than what is observed. This effect, along with the bimodal nature of the kinetic energy distribution for the static Coulomb explosion channel, has been previously observed by Bañares and co-workers at comparable laser intensities.[57] Their one-dimensional wavepacket calculations on *ab initio* potential energy curves of CH_3I^{2+} indicate that the lower KER observed experimentally is due to the partially bound nature of CH_3I^{2+}, while the bimodal energy distribution arises from the different electronic states of I^+ produced in the explosion. The two bands, centered at 4.46 ± 0.25 eV and 3.80 ± 0.13 eV, agree well with energies of two bands reported by Bañares and co-workers, 4.68 eV and 3.94 eV. The existence of a small CH_3I^{2+} peak in the time-of-flight spectrum of the experiment (Fig. 2) could also be further evidence for the dication showing some stability on the microsecond time scale of the experiment.

The very low kinetic energy feature (labeled III in Fig. 4) is assigned to multiphoton dissociative ionization induced by either the pump or probe pulses,[58–60]

$$\text{III}: \quad CH_3I \xrightarrow{nh\nu} CH_3^+ + I. \quad (3)$$

Dissociative ionization induced by the pump pulse, followed by ionization of the neutral cofragment by the probe pulse, also gives rise to a weak pump-probe delay-dependent feature (labeled IV in Fig. 4),[15]

$$\text{IV}: \quad CH_3I \xrightarrow{nh\nu\ 272\,\text{nm}} CH_3^+ + I \xrightarrow{nh\nu\ 815\,\text{nm}} CH_3^+ + I^+. \quad (4)$$

This assignment is supported by simple classical simulations (as described in detail in Sec. III A 2) using the measured kinetic energy releases of Channel III.

Finally, the sharp feature centered at 1.07 ± 0.05 eV (labeled V in Fig. 4) closely matches the 1.14 eV of the neutral photodissociation I^* channel at 266 nm.[25] This feature appears approximately after time-zero and its kinetic energy

shows no delay dependence, suggesting it arises due to ionization of a methyl fragment in the absence of a charged iodine co-fragment,

$$\text{V}: \quad CH_3I \xrightarrow{h\nu\ 272\,\text{nm}} CH_3 + I^* \xrightarrow{nh\nu\ 815\,\text{nm}} CH_3^+ + I^*. \quad (5)$$

This assignment is supported by recent coincidence experiments in which the feature is present in raw data, but disappears when considering only events in which CH_3^+ and I^+ are detected in coincidence.[61] A weaker feature corresponding to dissociation to a ground-state iodine would also be expected at approximately 1.9 eV, but is likely masked by the Ia and Ib channels.[55]

2. Analysis and simulation

For the delay-dependent channels discussed above, the total kinetic energy of the products, T, is

$$T = h\nu - D_0 - E^*_{\text{int}} - E_{\text{so}} + \frac{k_e q_A q_B}{r_{AB}}, \quad (6)$$

where D_0 is the C–I bond dissociation energy, E^*_{int} is the internal energy excitation of the products, and E_{so} is the spin-orbit splitting energy of the iodine. The final term accounts for the Coulombic repulsion, where k_e is the Coulomb constant, q_A and q_B are the charges on fragments A and B, and r_{AB} is the distance between them. As D_0 and E_{so} are known for CH_3I (2.41 eV and 0.943 eV, respectively[25]), the product internal energy excitation can be calculated from the asymptotic kinetic energies of the delay-dependent channels.[17]

The two delay-dependent channels in the CH_3^+ images (Ia and Ib) can be very simply modelled under the assumption that the absorption of the UV photon instantaneously accelerates the two fragments to their final velocities.[17] Given the photodissociation lifetime of approximately 100 fs,[26] any deviations from this behavior cannot be clearly observed in the experiment. In this case, the nuclear separation of the two charges as a function of pump-probe delay, t, is given by

$$r_{AB} = r_{\text{eq, AB}} + v_{\text{rel}} t, \quad (7)$$

where $r_{\text{eq,AB}}$ is the equilibrium separation of the charge centres in the undissociated molecule, v_{rel} is the relative velocity of the fragments resulting from the photodissociation, and t is the pump-probe delay time. It then follows that the total fragment kinetic energy is given by

$$T = T_{\text{UV}} + \frac{k_e q_A q_B}{r_{\text{eq, AB}} + v_{\text{rel}} t}, \quad (8)$$

where T_{UV} is the total UV-induced kinetic energy. From conservation of momentum, the individual fragment kinetic energies are related by

$$T_A = \frac{m_B}{m_A + m_B} T \quad \text{and} \quad T_B = \frac{m_A}{m_A + m_B} T. \quad (9)$$

Panel (a) in Fig. 5 shows the results of applying the above model for each experimental delay time from 20 fs onwards using the literature values for the initial bond length[56] (214 pm) and the final fragment velocities.[23] It can be seen that the simulated curve matches the experimental data well at late delay times, but at earlier delays, the agreement is poor, with the kinetic energies significantly overestimated. This implies that the observed internuclear separations at short pump-probe delays are greater than those simulated, and so the Coulomb explosion releases less energy than expected.

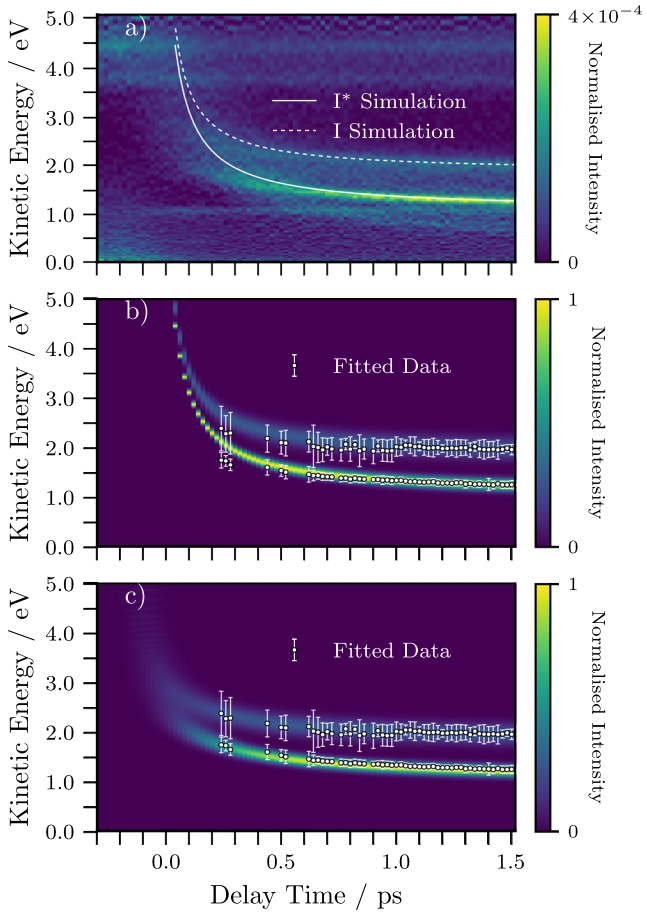

FIG. 5. Pump-probe delay-dependent features in the CH_3^+ kinetic energy distribution: (a) experimental data overlaid with simulations assuming a single final fragment velocity and including no timing convolution superimposed over the experimental heatmap; (b) simulated data accounting for the spread in final fragment velocities with no timing convolution; (c) simulated data accounting for the spread of final fragment velocities, with a timing convolution applied. Fitted experimental kinetic energies for channels IIa and IIb are superimposed over the simulated heatmaps, with error bars representing the FWHM of the Gaussian fits of each kinetic energy spectrum.

This effect can be explained by considering the temporal profiles of the pulses used in the experiment. The temporal resolution of the experiment was estimated to be approximately 280 fs from the observed cross correlations. In order to observe a pump-probe delay, the molecule must absorb a UV photon before undergoing ionization and subsequent Coulomb explosion by the IR pulse. This effect is particularly pronounced because the pump step requires only the absorption of a single UV photon and because the UV pulse is significantly longer than the IR pulse. For example, at the nominal time zero, the multiphoton absorption of the probe pulse is centered rather sharply at zero, while the probability to absorb a single UV photon follows the temporal shape of the pulse. This means that, at time zero (and, analogously, at all other delays), only the "early half" of the pump pulse actually contributes to the delay-dependent ion signal. This effectively causes a shift of

the observed signal towards the left because the most likely time of the UV photoabsorption is not centered at zero. The Coulomb explosions are therefore initiated at an increased internuclear separation on average, and so the overall KER is lower than would be expected. This effect is most notable at short delays, where the experiment is the most sensitive to nuclear separations due to the r^{-1} proportionality of the Coulombic repulsion.

To test the above argument, the simulations were convolved with the temporal resolution of the experiment. First, simulations were carried out on a series of final kinetic energies, representing the range of observed kinetic energies released by the photodissociation. A Gaussian convolution was then added to the pump-probe delay used in these calculations at each delay step. The results of these simulations without and with the timing convolution can be seen in Figs. 5(b) and 5(c), respectively. Experimental data from Gaussian fits of the two channels are superimposed over the simulations. Applying the convolution results in a far better agreement with the experimental data at shorter delay times. It is therefore expected that the use of shorter pulses would greatly diminish the level of blurring and allow for fast processes occurring over small nuclear displacements to be studied more clearly using time-resolved CEI.

B. Chloroiodomethane

1. Primary dissociation

Delay-dependent kinetic energy distributions of the I^+ and CH_2Cl^+ fragments of CH_2ClI are shown in Figs. 6(a) and 6(b).

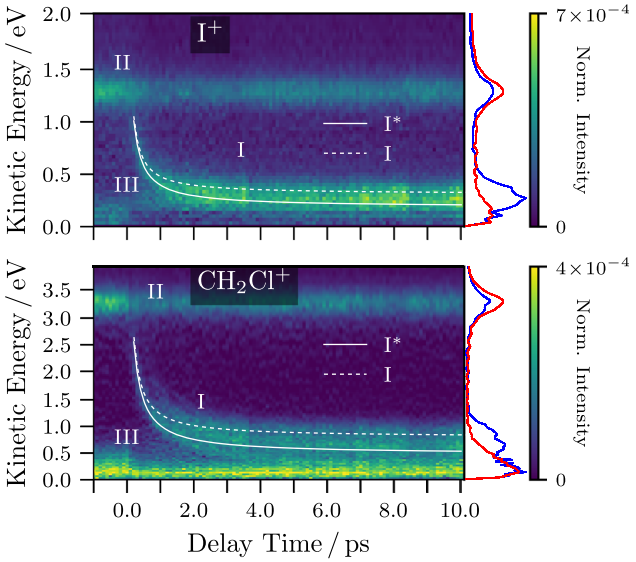

FIG. 6. Kinetic energy distributions as a function of pump-probe delay for the I^+ (top) and CH_2Cl^+ (bottom) ions, obtained from pbasex Abel inverted ion images. The kinetic energy spectrum for delays of +9.9 ps to +10.1 ps is projected to the right of each panel in blue. The kinetic energy spectrum for delays of −1.0 ps to −0.8 ps, in which the IR probe pulse arrives first, is projected in red. Simulated curves for the $I^*(^2P_{1/2})$ (I^*, white solid line) and $I(^2P_{3/2})$ (I, white dashed line) dissociation pathways are superimposed over the experimental data. These were modelled by assuming the fragments were instantly accelerated to their final velocities following neutral photodissociation, as described in the main text.

Three features can be identified in both data-sets, one of which has a kinetic energy that varies with pump-probe delay. This channel (labeled I in Fig. 6) again arises from sequential C–I cleavage and Coulomb explosion. Unlike in CH_3I, the two spin-orbit levels of the iodine product could not be resolved because the energy release is now shared more equally by the two fragments, as opposed to the CH_3I case, in which the lighter methyl fragment received almost all of the kinetic energy. Furthermore, there is a far greater degree of internal excitation following the photodissociation, which reduces the kinetic energy differences between the two product channels and broadens the observed kinetic energy distributions.

The kinetic energies of the delay-dependent channel at the maximum delay (+10.1 ps) for the I^+ and CH_2Cl^+ fragments are 0.27 ± 0.12 eV and 0.63 ± 0.30 eV. Subtracting the estimated Coulombic contribution from these energies gives values of 0.25 ± 0.12 eV and 0.58 ± 0.30 eV, in good agreement with the expected value of 0.23 eV for I^+, assuming the same energy partitioning as at 266 nm.[28]

The static (probe only) Coulomb explosion channel of the parent molecule (labeled II) is centered at 1.26 ± 0.10 eV and at 3.23 ± 0.20 eV for the I^+ and CH_2Cl^+ fragments, respectively. Assuming the charges are located on the I and Cl atoms, with the literature bond lengths and angles,[62] the calculated KERs are 1.26 eV and 3.24 eV for the two fragments, respectively. This strong level of agreement implies that in CH_2ClI, the Coulomb explosion is swift, with the two positive charges residing predominantly on the halogen atoms, and that it occurs prior to significant distortion of the molecular dication. The low kinetic energy channel (labeled III) is again assigned to multiphoton dissociative ionization.

The superimposed curves for delay times of 100 fs onwards were simulated with the previously described model using the literature values of the asymptotic velocities.[28] The experimental kinetic energy release peaks in the middle of the simulated I and I^* channels, which is consistent with a I:I^* branching ratio of roughly 1:1.[29] As the relative velocity of the two fragments following photodissociation is smaller than for CH_3I, and the kinetic energy distribution of the neutral photodissociation products is much broader, the temporal blurring effects discussed earlier have less influence in this experiment. Additionally, the initial separation between the two charged sites is approximately 50% greater in CH_2ClI^{2+} than in CH_3I^{2+}, and so due to the r^{-1} dependence of the Coulombic repulsion, the CH_3I system is more sensitive to any temporal blurring.

2. Recoil-frame covariance imaging

Multi-mass imaging facilitates the determination of correlations between ion momenta using coincidence or covariance analysis.[48] Recoil-frame covariance maps, as described in detail elsewhere,[14,49,51,63] are shown in Fig. 7 as examples. Here, the covariance maps represent the measured crushed velocity distribution of CH_2Cl^+ with respect to I^+, whose velocity is constrained vertically as illustrated.

Figure 7 shows covariance maps for pairs of fragment ions integrated over several pump-probe delay ranges. In the

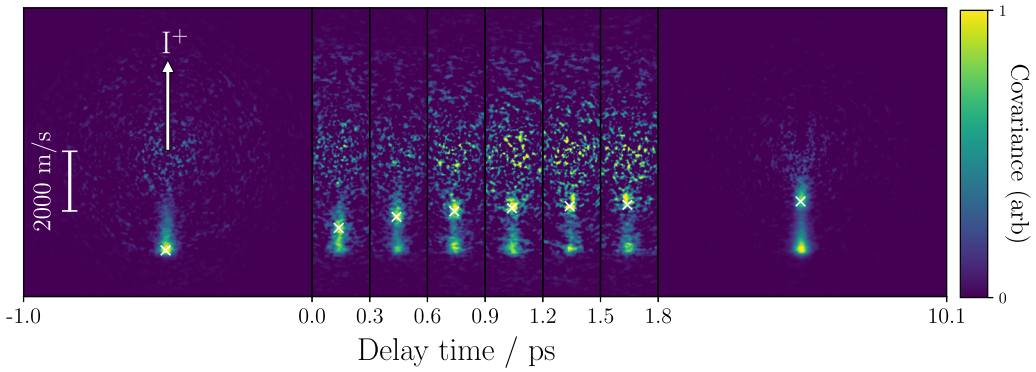

FIG. 7. Recoil-frame covariance maps for CH_2Cl^+, plotted with respect to an I^+ reference ion. These maps represent the crushed radial distribution of CH_2Cl^+ ions with respect to the velocity of I^+, which is constrained to a vector pointing directly upwards in these images, as represented by the white arrow. Covariance maps are integrated over the range of delays shown, i.e., −1.0 to 0 ps for the first image, 0 to +0.3 ps for the second, and so on. For images in the delay range 0 to +1.8 ps only a central portion of the image is shown to highlight the features discussed in the text. For positive delay times, the calculated KER (see the text) is indicated with a white cross, as is the calculated KER for the probe-only channel in the negative delay time image.

first image, shown in the left-most panel, corresponding to delay times in which the IR probe pulse arrives first, one high velocity feature can be seen clearly at a recoil angle of 180° from the I^+ reference (the vertical direction in the figure). This arises due to the probe-only Coulomb explosion of CH_2ClI (channel II in Fig. 6) and shows that the resulting I^+ and CH_2Cl^+ are produced in opposite directions from one another, as dictated by momentum conservation. In the covariance maps integrated over positive pump-probe delays, in which the UV pump pulse arrives first, an additional lower velocity feature arises. This is due to the photodissociation-Coulomb explosion channel (I in Fig. 6), in which the resulting ions again recoil with back-to-back velocities. This feature moves towards the centre of the image with increasing pump-probe delay, consistent with the decreasing kinetic energy shown in Fig. 6, further confirming this assignment. The images integrated over 300 fs delay ranges between 0 and 1.8 ps (for which only the central portion is shown for concision) correspond to just ≈1500 laser shots each and are somewhat noisy due to the limited statistics. This is in contrast to the very clean images for the earliest and latest delay ranges (at which point channel I is very close to its asymptotic energy), which were accumulated over ≈5000 and 40 000 laser shots, respectively. Despite the limited statistics, the two features can be clearly distinguished in these images, with the pump-probe channel varying radially with delay as expected. This demonstrates the efficacy of recoil-frame covariance analysis in time-resolved experiments, even when limited experimental time (such as at user facilities) restricts the amount of data which can be recorded for a given pump-probe delay. Additionally, as these covariance maps only show features arising from processes in which CH_2Cl^+ and I^+ are produced in coincidence, they can be used to support the assignments made in the raw images. For instance, the prominent lower kinetic energy feature seen in the CH_2Cl^+ images (channel III in Fig. 6) is absent in Fig. 7, supporting the assignment of dissociative ionization to give CH_2Cl^+ and neutral I fragments.

As CEI coupled with recoil-frame covariance analysis has been previously used to determine the structures of several complex polyatomic molecules,[7,49,50] the ability to determine clear covariances in pump-probe time-resolved experiments should allow for a wide range of structural changes initiated by a pump pulse to be accurately monitored in real-time.[49]

3. Three-body dissociation

The delay-dependent fragment energies of CH_2^+, Cl^+, and CH_2I^+ allow other dissociation pathways involving the cleavage of the C–Cl bond to be explored. Figure 8 shows the delay-dependent kinetic energies of these fragments. Delay-dependent features can be observed in the kinetic energies of CH_2^+ and Cl^+, whilst no such feature can be seen for CH_2I^+, which is solely produced with a very low kinetic energy (<0.3 eV) at all delay times. The lack of any delay-dependent feature in the CH_2I^+ suggests that the primary C–Cl bond cleavage is an unlikely process at the excitation wavelength employed (272 nm), supporting the conclusions of previous studies.[30] This mirrors the behavior of CH_2BrI, in which primary C–Br cleavage at 272 nm also rarely occurs.[17,39]

The lack of any delay-dependent feature in the CH_2I^+ indicates that the feature seen in the Cl^+ map instead arises from a dissociation that cleaves both carbon-halogen bonds in either a sequential or concerted process. The energy required for this is 6.78 eV.[64] As the photon energy of the pump pulse is only 4.57 eV, the three-body dissociation must follow the absorption of at least two UV photons. Figure 8 shows simulated Coulomb explosion curves for this process, assuming no internal excitation of the nascent CH_2^+ fragment and the absorption of two UV photons. The two halogen atoms were assumed to recoil immediately along the carbon-halogen bond axes, with the CH_2 recoil velocity given by momentum conservation. Simulated curves in which either two or three of the resulting fragments are ionized by the probe pulse are displayed. The agreement between the observed and simulated curves is qualitatively good, particularly at long delay times. This agreement at long delay times, where the Coulombic contribution to the kinetic energy releases is minimal, suggests that the observed features arise from three-body dissociation following absorption of two UV photons and that there is little internal energy excitation in the CH_2 fragment. This is to be expected, given studies of the analogous process in CH_2BrI, in

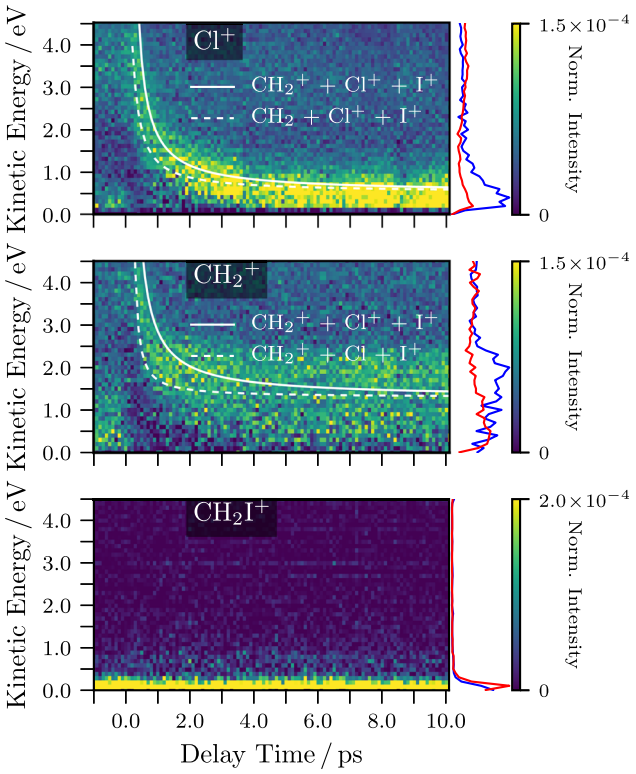

FIG. 8. Kinetic energy distributions as a function of pump-probe delay for the Cl^+ (top), CH_2^+ (middle), and CH_2I^+ (bottom) ions, obtained from pBASEX Abel inverted ion images. The kinetic energy spectrum for delays of +9.9 ps to +10.1 ps is projected to the right of each panel in blue. The kinetic energy spectrum for delays of −1.0 ps to −0.8 ps, in which the IR probe pulse arrives first, is projected in red. Simulated curves for secondary dissociation followed by ionization of two or three fragments by the probe pulse are superimposed over the experimental data. These were modelled assuming the fragments were instantly accelerated to their final velocities following neutral photodissociation, as described in the main text.

which only 11.6% of the available energy was partitioned into internal modes.[17,39] It should also be noted that the images for the CH_2^+ and Cl^+ fragments fill, and may exceed, the detector, and so the high KER feature at short delays may not be fully captured. It is also possible that other processes may contribute to the broad delay-dependent features observed, such as dissociative ionizations followed by Coulomb explosion. However, given that the asymptotic kinetic energies of the pump-probe channels exceed that of the low energy dissociative ionization channels observed before time-zero, we can assign the majority of the pump-probe effects to the three-body dissociation as discussed.

TABLE I. Fraction of the available energy partitioned as internal energy of the polyatomic cofragment, $f_{int} = E_{int}/E_{avail}$, where E_{int} is the internal energy of the fragments and E_{avail} is the available energy following dissociation.

Molecule	f_{int} (this work)	f_{int} (references)
CH_3I	6.4% ± 0.9% (I channel) 2.8% ± 0.6% (I*channel)	4.6% (I channel) (Ref. 23) 2.5% (I* channel) (Ref. 23)
CH_2ClI	54.3% ± 1.1%	55% (Ref. 28)
CH_2BrI	65.6% ± 1.6% (Ref. 17)	68% (Ref. 39)

C. Comparison of CH_2BrI, CH_2ClI, and CH_3I

Comparing the two halomethanes studied in this work with the results recently published from analogous studies on the CH_2BrI molecule,[17] the effects of substitution of a second halogen atom on the energy partitioning following primary photodissociation can be clearly observed. Table I provides values for the proportion of energy released in the C–I dissociation into internal modes of the radical cofragment. These values were extracted from the kinetic energy releases in the final pump-probe delays in each experiment and corrected for any calculated residual Coulomb repulsion.

It can be clearly seen that in the disubstituted halomethanes, the amount of energy partitioning into internal modes is far greater than in the CH_3I case. Additionally, there is greater internal energy excitation in CH_2Br than in CH_2Cl. Previous detailed studies on the CH_3I molecule have shown that the umbrella vibrational mode of the CH_3 fragment is only slightly excited,[25] with very little rotational excitation of the methyl radical. It can be assumed that the increased internal excitation in the geminal dihaloalkanes is predominantly partitioned into rotation, consistent with recent femtosecond REMPI-VMI experiments.[65]

These observations can be understood through considering a very simple classic model of the photodissociation of these molecules, as depicted in Fig. 9. In moving from CH_3I to CH_2ClI to CH_2BrI, the centre of mass of the polyatomic product moves further away from the C–I bond axis, upon which one would expect any momentum released in the dissociation to be directed. As a result, a greater classical torque is applied to the recoiling polyatomic cofragment, causing a greater degree of rotational excitation. Calculations of the centre of masses of the recoiling radicals indicate the classical torque imparted is approximately 30% greater in the dissociation of CH_2BrI relative to CH_2ClI, agreeing well with the observed internal energy distributions.

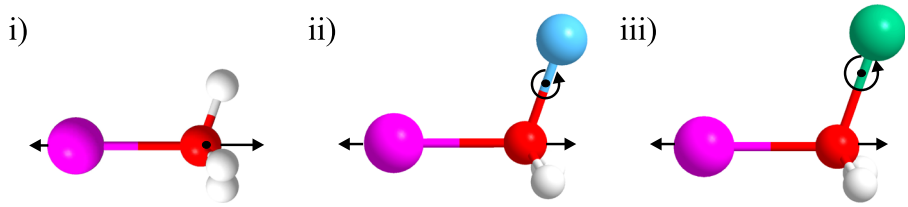

FIG. 9. Schematic of the photodissociation of (i) CH_3I, (ii) CH_2ClI, and (iii) CH_2BrI showing the centre of mass of each of the resulting polyatomic fragments following C–I photodissociation. C, H, I, Br, and Cl atoms are coloured red, gray, purple, green, and blue, respectively. In CH_3I, the centre of mass lies along the vector of the momentum induced by the dissociation. In CH_2ClI and CH_2BrI, the centre of mass is significantly displaced from this vector, and so a large torque is applied to the recoiling fragment.

IV. CONCLUSIONS AND OUTLOOK

Results from experiments in which time-dependent CEI was used in conjunction with a fast time-stamping detector to explore the photodissociation dynamics of iodomethane and iodochloromethane were presented. In the *A*-band dissociation of CH_3I, two different reaction pathways corresponding to different final iodine spin-orbit states could be clearly distinguished in a time-resolved manner during a single experiment. In the geminal dihaloalkane CH_2ClI, primary and secondary dissociations could be studied simultaneously, yielding results in good agreement with the literature.

The presented results show the potential of time-resolved CEI in elucidating photochemical reaction mechanisms. The universal nature of the probe greatly extends the number of applicable molecules compared to traditional REMPI-VMI experiments. Time-resolved recoil-frame covariance imaging, as demonstrated here, could be used to study the detailed structural dynamics of more complex photochemistry. It could, in principle, be applied to follow the nuclear motion taking place during ring-opening reactions[66,67] or *cis-trans* isomerisation reactions,[68–70] which are often very challenging to study in the gas phase using traditional spectroscopic techniques.

SUPPLEMENTARY MATERIAL

See supplementary material for a listing of the author contributions.

ACKNOWLEDGMENTS

The authors gratefully acknowledge the work of the scientific and technical team at FLASH, especially the FLASH laser group who made these experiments possible. We acknowledge the Max Planck Society for funding the development and the initial operation of the CAMP end-station within the Max Planck Advanced Study Group at CFEL and for providing this equipment for CAMP@FLASH. The installation of CAMP@FLASH was partially funded by the BMBF grants Nos. 05K10KT2, 05K13KT2, 05K16KT3 and 05K10KTB from FSP-302. The M.B., C.V., and S.R.M. groups are grateful for the support of the UK EPSRC (Programme Grant Nos. EP/G00224X/1 and EP/L005913/1), the EU (FP7 ITN "ICONIC," Project No. 238671), and the STFC (PNPAS award and mini-IPS Grant No. ST/J002895/1). F.A. additionally thanks Magdalen College, Oxford for their support. A.R. and D.R. acknowledge support from the Chemical Sciences, Geosciences, and Biosciences Division, Office of Basic Energy Sciences, Office of Science, U.S. Department of Energy, Grant No. DE-FG02-86ER13491. D.R., E.S., R.B., C.B., and B.E. were also supported by the Helmholtz Gemeinschaft through the Helmholtz Young Investigator Program, and R.B. and S.T. are additionally grateful for financial support from the German Research Council (DFG), CRC 755 (Project No. B03) and CRC 1073 (Project No. C02). J.K., S. T., and J.W. acknowledge support from the excellence cluster "The Hamburg Center for Ultrafast Imaging—Structure, Dynamics and Control of Matter at the Atomic Scale" of the Deutsche Forschungsgemeinschaft (CUI, DFG-EXC1074) and the European Research Council under the European Union's Seventh Framework Programme (No. FP7/2007-2013) through the Consolidator Grant COMOTION (No. ERC-Küpper-614507). J.K. and S.B. thank the Initiative and Networking Fund of the Helmholtz Association and the DFG (No. CRC 755/B03). The support of the EU to J.K., P.J., J.L., H.S., and D.R. via the MEDEA project within the Horizon 2020 research and innovation programme under the Marie Skłodowska-Curie grant agreement (No. 641789) is also gratefully acknowledged. A.S.M. and P.K.O. thank the German-Russian Interdisciplinary Science Center (G-RISC, C-2015a-6, C-2015b-6, and C-2016b-7) funded by the German Federal Foreign Office via the German Academic Exchange Service (DAAD). J.L., S.M., and P.J. thank the Swedish Research Council and the Swedish Foundation for Strategic Research. T.M. acknowledges financial support from the French Agence Nationale de la Recherche (ANR) through the ATTOMEMUCHO project (No. ANR-16-CE30-0001). A.R. is grateful for support through the Deutsche Forschungsgemeinschaft (DFG Grant No. RO 4577/1-1). The group from Sorbonne Université acknowledges the PICS and XFEL PEPS financial support program from CNRS.

[1] A. H. Zewail, J. Phys. Chem. A **104**, 5660 (2000).
[2] J. H. Posthumus, Rep. Prog. Phys. **67**, 623 (2004).
[3] Z. Vager, R. Namaan, and E. P. Kanter, Science **244**, 426 (1989).
[4] H. Stapelfeldt, E. Constant, H. Sakai, and P. B. Corkum, Phys. Rev. A **58**, 426 (1998).
[5] M. Pitzer, M. Kunitski, A. S. Johnson, T. Jahnke, H. Sann, F. Sturm, L. P. H. Schmidt, H. Schmidt-Böcking, R. Dörner, J. Stohner, J. Kiedrowski, M. Reggelin, S. Marquardt, A. Schießer, R. Berger, and M. S. Schöffler, Science **341**, 1096 (2013).
[6] U. Ablikim, C. Bomme, H. Xiong, E. Savelyev, R. Obaid, B. Kaderiya, S. Augustin, K. Schnorr, I. Dumitriu, T. Osipov, R. Bilodeau, D. Kilcoyne, V. Kumarappan, A. Rudenko, N. Berrah, and D. Rolles, Sci. Rep. **6**, 38202 (2016).
[7] M. Burt, K. Amini, J. W. L. Lee, L. Christiansen, R. R. Johansen, Y. Kobayashi, J. D. Pickering, C. Vallance, M. Brouard, and H. Stapelfeldt, J. Chem. Phys. **148**, 091102 (2018).
[8] H. Stapelfeldt, E. Constant, and P. B. Corkum, Phys. Rev. Lett. **74**, 3780 (1995).
[9] T. Ergler, A. Rudenko, B. Feuerstein, K. Zrost, C. D. Schröter, R. Moshammer, and J. Ullrich, Phys. Rev. Lett. **95**, 093001 (2005).
[10] F. Légaré, K. F. Lee, A. D. Bandrauk, D. M. Villeneuve, and P. B. Corkum, J. Phys. B: At., Mol. Opt. Phys. **39**, S503 (2006).
[11] T. Ergler, A. Rudenko, B. Feuerstein, K. Zrost, C. D. Schröter, R. Moshammer, and J. Ullrich, J. Phys. B: At., Mol. Opt. Phys. **39**, S493 (2006).
[12] I. A. Bocharova, A. S. Alnaser, U. Thumm, T. Niederhausen, D. Ray, C. L. Cocke, and I. V. Litvinyuk, Phys. Rev. A **83**, 013417 (2011).
[13] A. Rouzée, P. Johnsson, L. Rading, A. Hundertmark, W. Siu, Y. Huismans, S. Düsterer, H. Redlin, F. Tavella, N. Stojanovic, A. Al-Shemmary, F. Lépine, D. M. P. Holland, T. Schlatholter, R. Hoekstra, H. Fukuzawa, K. Ueda, and M. J. J. Vrakking, J. Phys. B: At., Mol. Opt. Phys. **46**, 164029 (2013).
[14] L. Christensen, J. H. Nielsen, C. B. Brandt, C. B. Madsen, L. B. Madsen, C. S. Slater, A. Lauer, M. Brouard, M. P. Johansson, B. Shepperson, and H. Stapelfeldt, Phys. Rev. Lett. **113**, 073005 (2014).
[15] B. Erk, R. Boll, S. Trippel, D. Anielski, L. Foucar, B. Rudek, S. W. Epp, R. Coffee, S. Carron, S. Schorb, K. R. Ferguson, M. Swiggers, J. D. Bozek, M. Simon, T. Marchenko, J. Küpper, I. Schlichting, J. Ullrich, C. Bostedt, D. Rolles, and A. Rudenko, Science **345**, 288 (2014).
[16] R. Boll, B. Erk, R. Coffee, S. Trippel, T. Kierspel, C. Bomme, J. D. Bozek, M. Burkett, S. Carron, K. R. Ferguson, L. Foucar, J. Küpper, T. Marchenko, C. Miron, M. Patanen, T. Osipov, S. Schorb, M. Simon, M. Swiggers, S. Techert, K. Ueda, C. Bostedt, D. Rolles, and A. Rudenko, Struct. Dyn. **3**, 043207 (2016).
[17] M. Burt, R. Boll, J. W. L. Lee, K. Amini, H. Köckert, C. Vallance, A. S. Gentleman, S. R. Mackenzie, S. Bari, C. Bomme, S. Düsterer, B. Erk, B. Manschwetus, E. Müller, D. Rompotis, E. Savelyev, N. Schirmel, S. Techert, R. Treusch, J. Küpper, S. Trippel, J. Wiese, H. Stapelfeldt, B. C. de Miranda, R. Guillemin, I. Ismail, L. Journel, T. Marchenko, J. Palaudoux,

F. Penent, M. N. Piancastelli, M. Simon, O. Travnikova, F. Brausse, G. Goldsztejn, A. Rouzée, M. Géléoc, R. Geneaux, T. Ruchon, J. Underwood, D. M. P. Holland, A. S. Mereshchenko, P. K. Olshin, P. Johnsson, S. Maclot, J. Lahl, A. Rudenko, F. Ziaee, M. Brouard, and D. Rolles, Phys. Rev. A **96**, 043415 (2017).
[18]S. J. Riley and K. R. Wilson, Faraday Discuss. Chem. Soc. **53**, 132 (1972).
[19]M. O. Hale, G. E. Galica, S. G. Glogover, and J. L. Kinsey, J. Phys. Chem. **90**, 4997 (1986).
[20]Q. Zhu, J. R. Cao, Y. Wen, J. Zhang, X. Zhong, Y. Huang, W. Fang, and X. Wu, Chem. Phys. Lett. **144**, 486 (1988).
[21]D. W. Chandler, J. W. Thoman, Jr., M. H. M. Janssen, and D. H. Parker, Chem. Phys. Lett. **156**, 151 (1989).
[22]Y. Amatatsu, K. Morokuma, and S. Yabushita, J. Chem. Phys. **94**, 4858 (1991).
[23]A. T. J. B. Eppink and D. H. Parker, J. Chem. Phys. **109**, 4758 (1998).
[24]D. P. Zhong and A. H. Zewail, J. Phys. Chem. A **102**, 4031 (1998).
[25]A. T. J. B. Eppink and D. H. Parker, J. Chem. Phys. **110**, 832 (1999).
[26]R. de Nalda, J. G. Izquierdo, J. Durá, and L. Bañares, J. Chem. Phys. **126**, 021101 (2007).
[27]F. Braußе, G. Goldsztejn, K. Amini, R. Boll, S. Bari, C. Bomme, M. Brouard, M. Burt, B. C. de Miranda, S. Düsterer, B. Erk, M. Géléoc, R. Geneaux, A. S. Gentleman, R. Guillemin, I. Ismail, P. Johnsson, L. Journel, T. Kierspel, H. Köckert, J. Küpper, P. Lablanquie, J. Lahl, J. W. L. Lee, S. R. Mackenzie, S. Maclot, B. Manschwetus, A. S. Mereshchenko, T. Mullins, P. K. Olshin, J. Palaudoux, S. Patchkovskii, F. Penent, M. N. Piancastelli, D. Rompotis, T. Ruchon, A. Rudenko, E. Savelyev, N. Schirmel, S. Techert, O. Travnikova, S. Trippel, J. G. Underwood, C. Vallance, J. Wiese, M. Simon, D. M. P. Holland, T. Marchenko, A. Rouzée, and D. Rolles, Phys. Rev. A **97**, 043429 (2018).
[28]M. L. Murillo-Sánchez, S. Marggi Poullain, J. González-Vázquez, M. E. Corrales, G. Balerdi, and L. Bañares, Chem. Phys. Lett. **683**, 22 (2017).
[29]D. Senapati and P. K. Das, Chem. Phys. Lett. **393**, 535 (2004).
[30]D. Senapati, K. Kavita, and P. K. Das, J. Phys. Chem. A **106**, 8479 (2002).
[31]T. Zhang, C. Y. Ng, F. Qi, C.-S. Lam, and W.-K. Li, J. Chem. Phys. **123**, 174316 (2005).
[32]G. Schmitt and F. J. Comes, J. Photochem. Photobiol., A **41**, 13 (1987).
[33]L. Rubio-Lago, A. García-Vela, A. Arregui, G. A. Amaral, and L. Bañares, J. Chem. Phys. **131**, 174309 (2009).
[34]S. H. Gardiner, M. L. Lipciuc, T. N. V. Karsili, M. N. R. Ashfold, and C. Vallance, Phys. Chem. Chem. Phys. **17**, 4096 (2015).
[35]A. G. Sage, T. A. A. Oliver, D. Murdock, M. B. Crow, G. A. D. Ritchie, J. N. Harvey, and M. N. R. Ashfold, Phys. Chem. Chem. Phys. **13**, 8075 (2011).
[36]K. Kavita and P. K. Das, J. Chem. Phys. **117**, 2038 (2002).
[37]M. Cheng, D. Lin, L. Hu, Y. Du, and Q. Zhu, Phys. Chem. Chem. Phys. **18**, 3165 (2016).
[38]S. J. Lee and R. Bersohn, J. Phys. Chem. **86**, 728 (1982).
[39]L. J. Butler, E. J. Hintsa, S. F. Shane, and Y. T. Lee, J. Chem. Phys. **86**, 2051 (1987).
[40]L. Strüder, S. Epp, D. Rolles, R. Hartmann, P. Holl, G. Lutz, H. Soltau, R. Eckart, C. Reich, K. Heinzinger, C. Thamm, A. Rudenko, F. Krasniqi, K.-U. Kühnel, C. Bauer, C.-D. Schröter, R. Moshammer, S. Techert, D. Miessner, M. Porro, O. Hälker, N. Meidinger, N. Kimmel, R. Andritschke, F. Schopper, G. Weidenspointner, A. Ziegler, D. Pietschner, S. Herrmann, U. Pietsch, A. Walenta, W. Leitenberger, C. Bostedt, T. Möller, D. Rupp, M. Adolph, H. Graafsma, H. Hirsemann, K. Gärtner, R. Richter, L. Foucar, R. L. Shoeman, I. Schlichting, and J. Ullrich, Nucl. Instrum. Methods Phys. Res., Sect. A **614**, 483 (2010).
[41]D. Rolles, R. Boll, M. Adolph, A. Aquila, C. Bostedt, J. D. Bozek, H. N. Chapman, R. Coffee, N. Coppola, P. Decleva, T. Delmas, S. W. Epp, B. Erk, F. Filsinger, L. Foucar, L. Gumprecht, A. Hömke, T. Gorkhover, L. Holmegaard, P. Johnsson, C. Kaiser, F. Krasniqi, K.-U. Kühnel, J. Maurer, M. Messerschmidt, R. Moshammer, W. Quevedo, I. Rajkovic, A. Rouzée, B. Rudek, I. Schlichting, C. Schmidt, S. Schorb, C. D. Schröter, J. Schulz, H. Stapelfeldt, M. Stener, S. Stern, S. Techert, J. Thøgersen, M. J. J. Vrakking, A. Rudenko, J. Küpper, and J. Ullrich, J. Phys. B: At., Mol. Opt. Phys. **47**, 124035 (2014).
[42]B. Erk, J. P. Müller, C. Bomme, R. Boll, G. Brenner, H. Chapman, J. Correa, S. Düsterer, S. Dziarzhytski, S. Eisebitt, H. Graafsma, S. Grunewald, L. Gumprecht, R. Hartmann, G. Hauser, B. Keitel, C. von Korff Schmising, M. Kuhlmann, B. Manschwetus, L. Mercadier, E. Müller, C. Passow, E. Plönjes, D. Ramm, D. Rompotis, A. Rudenko, D. Rupp, M. Sauppe, F. Siewert, D. Schlosser, L. Strüder, A. Swiderski, S. Techert, K. Tiedtke, T. Tilp, R. Treusch, I. Schlichting, J. Ullrich, R. Moshammer, T. Möller, and D. Rolles, J. Synchrotron Radiat. **25**, 1529 (2018).
[43]C. Bomme *et al.*, "A double sided velocity map imaging spectrometer optimized for high energy electron and ion coincidence measurements" (unpublished).
[44]H. Redlin, A. Al-Shemmary, A. Azima, N. Stojanovic, F. Tavella, I. Will, and S. Düsterer, Nucl. Instrum. Methods Phys. Res., Sect. A **635**, S88 (2011).
[45]A. T. J. B. Eppink and D. H. Parker, Rev. Sci. Instrum. **68**, 3477 (1997).
[46]A. Nomerotski, S. Adigun-Boaye, M. Brouard, E. Campbell, A. Clark, J. Crooks, J. John, A. Johnsen, C. Slater, R. Turchetta, C. Vallance, E. Wilman, and W. Yuen, Nucl. Instrum. Methods Phys. Res., Sect. A **633**, S243 (2011).
[47]J. J. John, M. Brouard, A. Clark, J. Crooks, E. Halford, L. Hill, J. W. L. Lee, A. Nomerotski, R. Pisarczyk, I. Sedgwick, C. S. Slater, R. Turchetta, C. Vallance, E. Wilman, B. Winter, and W. H. Yuen, J. Instrum. **7**, C08001 (2012).
[48]L. J. Frasinski, K. Codling, and P. A. Hatherly, Science **246**, 1029 (1989).
[49]C. S. Slater, S. Blake, M. Brouard, A. Lauer, C. Vallance, C. S. Bohun, L. Christensen, J. H. Nielsen, M. P. Johansson, and H. Stapelfeldt, Phys. Rev. A **91**, 053424 (2015).
[50]J. D. Pickering, K. Amini, M. Brouard, M. Burt, I. J. Bush, L. Christensen, A. Lauer, J. H. Nielsen, C. S. Slater, and H. Stapelfeldt, J. Chem. Phys. **144**, 161105 (2016).
[51]L. J. Frasinski, J. Phys. B: At., Mol. Opt. Phys. **49**, 152004 (2016).
[52]C. S. Slater, S. Blake, M. Brouard, A. Lauer, C. Vallance, J. J. John, R. Turchetta, A. Nomerotski, L. Christensen, J. H. Nielsen, M. P. Johansson, and H. Stapelfeldt, Phys. Rev. A **89**, 011401 (2014).
[53]G. A. Garcia, L. Nahon, and I. Powis, Rev. Sci. Instrum. **75**, 4989 (2004).
[54]D. Manura and D. Dahl, SIMION (R) 8.0, 2008.
[55]K. Amini, E. Savelyev, F. Braußе, N. Berrah, C. Bomme, M. Brouard, M. Burt, L. Christensen, S. Düsterer, B. Erk, H. Höppner, T. Kierspel, F. Krecinic, A. Lauer, J. W. L. Lee, M. Müller, E. Müller, T. Mullins, H. Redlin, N. Schirmel, J. Thøgersen, S. Techert, S. Toleikis, R. Treusch, S. Trippel, A. Ulmer, C. Vallance, J. Wiese, P. Johnsson, J. Küpper, A. Rudenko, A. Rouzée, H. Stapelfeldt, D. Rolles, and R. Boll, Struct. Dyn. **5**, 014301 (2018).
[56]L. E. Sutton, *Tables of Interatomic Distances and Configuration in Molecules and Ions: Supplement 1956-1959* (Chemical Society, 1965).
[57]M. E. Corrales, G. Gitzinger, J. González-Vázquez, V. Loriot, R. de Nalda, and L. Bañares, J. Phys. Chem. A **116**, 2669 (2012).
[58]P. C. Samartzis, B. L. G. Bakker, D. H. Parker, and T. N. Kitsopoulos, J. Phys. Chem. A **103**, 6106 (1999).
[59]Y. Wang, S. Zhang, Z. Wei, and B. Zhang, J. Phys. Chem. A **112**, 3846 (2008).
[60]D. Zhang, S. Luo, H. Xu, M. Jin, F. Liu, B. Yan, Z. Wang, H. Liu, D. Jiang, A. Eppink, W. Roeterdink, S. Stolte, and D. Ding, Eur. Phys. J. D **71**, 148 (2017).
[61]F. Ziaee and D. Rolles *et al.*, "Time-resolved coincident ion momentum imaging of the UV-induced dissociation of CH_3I" (unpublished).
[62]W. Gordy, J. W. Simmons, and A. G. Smith, Phys. Rev. **74**, 243 (1948).
[63]J. L. Hansen, J. H. Nielsen, C. B. Madsen, A. T. Lindhardt, M. P. Johansson, T. Skrydstrup, L. B. Madsen, and H. Stapelfeldt, J. Chem. Phys. **136**, 204310 (2012).
[64]M. W. Chase, Jr., J. Phys. Chem. Ref. Data Monogr. **9**, 1 (1998).
[65]M. L. Murillo-Sánchez, S. Marggi Poullain, J. J. Bajo, M. E. Corrales, J. González-Vázquez, I. R. Solá, and L. Bañares, Phys. Chem. Chem. Phys. **20**, 20766 (2018).
[66]V. S. Petrović, M. Siano, J. L. White, N. Berrah, C. Bostedt, J. D. Bozek, D. Broege, M. Chalfin, R. N. Coffee, J. Cryan, L. Fang, J. P. Farrell, L. J. Frasinski, J. M. Glownia, M. Gühr, M. Hoener, D. M. P. Holland, J. Kim, J. P. Marangos, T. Martinez, B. K. McFarland, R. S. Minns, S. Miyabe, S. Schorb, R. J. Sension, L. S. Spector, R. Squibb, H. Tao, J. G. Underwood, and P. H. Bucksbaum, Phys. Rev. Lett. **108**, 253006 (2012).
[67]M. P. Minitti, J. M. Budarz, A. Kirrander, J. S. Robinson, D. Ratner, T. J. Lane, D. Zhu, J. M. Glownia, M. Kozina, H. T. Lemke, M. Sikorski, Y. Feng, S. Nelson, K. Saita, B. Stankus, T. Northey, J. B. Hastings, and P. M. Weber, Phys. Rev. Lett. **114**, 255501 (2015).
[68]J. A. Syage, W. R. Lambert, P. M. Felker, A. H. Zewail, and R. M. Hochstrasser, Chem. Phys. Lett. **88**, 266 (1982).
[69]I. K. Lednev, T.-Q. Ye, R. E. Hester, and J. N. Moore, J. Phys. Chem. **100**, 13338 (1996).
[70]K. Ishii, S. Takeuchi, and T. Tahara, Chem. Phys. Lett. **398**, 400 (2004).